Published in final edited form as:
Anal Chem. 2007 December 1; 79(23): 9007–9013. doi:10.1021/ac7016597.

Polymer Microfluidic Chips with Integrated Waveguides for Reading Microarrays

Feng Xu[†,‡], **Proyag Datta**[§], **Hong Wang**[†,‡], **Sitanshu Gurung**[§], **Masahiko Hashimoto**[†,‡], **Suying Wei**[‡], **Jost Goettert**[§], **Robin L. McCarley**[†,‡], and **Steven A. Soper**[*,†,‡]
Department of Chemistry, Center for Bio-Modular Multi-Scale Systems (CBM^2), Center for Advanced Microstructure and Devices (CAMD), Louisiana State University, Baton Rouge, Louisiana 70803, U.S.A

Abstract

A microfluidic chip with an integrated planar waveguide was fabricated in poly(methyl methacrylate), PMMA, using a single-step, double-sided hot-embossing approach. The waveguide was embedded in air on three sides and the solution being interrogated on the fourth. DNA probes were covalently attached to the waveguide surface by plasma activating the PMMA and the use of carbodiimide coupling chemistry. Successful hybridization events were read using evanescent excitation monitored by an imaging microscope, which offered high spatial resolution (2 μm) and a large field-of-view (20-mm-diameter field-of-view), providing imaging of the entire array without scanning. The application of the microfluidic/waveguide assembly was demonstrated by detecting low abundant point mutations; insertion *C* mutations in *BRCA*1 genes associated with breast cancer were analyzed using a universal array coupled to an allele-specific ligation assay. DNA probes consisting of amine-terminated oligonucleotides were printed inside the microfluidic channel using a non-contact micro-spotter. Mutant and wide-type genomic DNAs of *BRCA*1 were PCR amplified, with the amplicons subjected to ligation detection reactions (LDRs). LDR solutions were allowed to flow over the microarray positioned on the polymer waveguide with successful ligation events discerned through fluorescence signatures present at certain locations of the array. The microfluidic/waveguide assembly could detect polymorphisms present at <1% of the total DNA content.

Keywords

Waveguide; Microarray; Microfluidics; Mutation detection; Breast cancer; Ligase detection reaction (LDR); Poly(methyl methacrylate)

INTRODUCTION

Readout of microarrays commonly uses a laser-induced fluorescence scanner, where a near diffraction-limited excitation area is sequentially rastered over the microarray surface. There are a number of companies that offer microarray scanners that typically consist of dual laser excitation (532 and 633 nm excitation wavelengths), scanning areas of 25 × 75 mm and spatial resolution down to approximately 5 μm (for example, see Agilent Technologies, www.agilent.com). The scanning time per microarray slide varies tremendously and depends on the scan resolution, integration time per step and the number of color channels.[1]

* To whom correspondence should be addressed. E-mail: chsope@lsu.edu 225-578-1527 (Phone), 225-578-3458 (Fax).
†Center for Bio-Modular Multi-Scale Systems, Louisiana State University. E-mail: fengxu@lsu.edu 225-578-5248 (Phone).
‡Department of Chemistry, Louisiana State University.
§Center for Advanced Microstructure and Devices, Louisiana State University.

An alternative strategy for reading fluorescence signatures from microarrays is to place the array on a planar waveguide and use evanescent excitation with the fluorescence transduced via an imaging detector, such as a CCD. The advantages of using waveguides as the microarray foundation is that they can guide light over several square centimeters allowing the irradiation of the entire array surface for image capture in a time period significantly less than that of a scanner. In addition, real-time monitoring of association events can be followed for performing kinetic analyses. However, waveguide-based arrays using imaging optics for readout can provide poorer limits of detection compared to scanning-type fluorescence detectors due to the use of high numerical aperture relay optics used in scanning formats. For guiding to occur, the refractive index of a core layer must be larger than that of its surrounding (*i.e.*, cladding).[2] When the guiding light is launched at or above the critical angle, total internal reflection occurs. The internally reflected rays produce a local evanescent field at the outer surface of the waveguide, which has an intensity that decays exponentially with distance from the waveguide surface.

The challenges with using planar waveguides for imaging molecular recognition events on microarrays is to build a guiding medium that can both support total internal reflection with a strong evanescent field and allow for the covalent attachment of recognition probes to its surface. Planar waveguides that satisfy the above criteria have been made from a variety of materials such as metal films,[3] photonic crystals (Ta_2O_5-SiO_2,[4, 5] GaAs-air bridged[6]), Si-SiO_2,[7] PDMS,[8] silicon oxynitride[9] and phosphorus doped silica cores with boron doped glass claddings.[10] In most cases, the guiding medium is deposited as a thin film on some type of support. Zeptosens has recently reported on a planar waveguide that consists of a 150 nm thin film of high refractive index material (Ta_2O_5) deposited onto a glass support, which has been used to read fluorescence signatures from DNA or protein microarrays.[5] While glass is one of the most commonly used material for waveguide applications,[11] it becomes problematic when considering to incorporate this optical element into other sample processing units, such as microfluidics, due to its limited fabrication modalities that make glass devices difficult to employ for one-time use formats required for *in vitro* diagnostics.

Another material that has created interest as a guiding material is polymers[12, 13] because of their low-cost and simple fabrication characteristics and in some cases, favorable optical properties.[14] A recent report highlighted the integration of a micromirror with a polymer-filled cavity to a microfluidic network using a multi-layered structure.[15] The cavity was etched with KOH into a low stress silicon nitride layer that was situated underneath a thin glass sheet with a PDMS microchannel reversibly sealed to the glass.

Integration of microarrays with microfluidics has several attractive features that can potentially circumvent limitations associated with conventional 2-dimensional arrays such as:[16] (1) Reductions in hybridization incubation time due to short diffusional distances;[17] (2) integration of sample preprocessing steps into the microfluidic system[18, 19] and; (3) an enclosed fluidic architecture that can reduce the potential of sample contamination.[20] However, the operational characteristics associated with the microarray in terms of the substrate including high optical clarity, minimal non-specific adsorption and robust linkage chemistries must be balanced with the microfabrication techniques used to produce the desired fluidic structures.

In this paper, we report on the integration of a poly(methyl methacrylate), PMMA, waveguide and DNA microarray into a microfluidic chip produced through a single-step, double-sided hot-embossing process. The double-sided embossing produced an air-embedded waveguide in PMMA with the top of the waveguide serving as the floor of the microfluidic channel. Oxygen plasma was used to activate the PMMA waveguide surface and when reacted with 1-(3-dimethylaminopropyl)-3-ethylcarbodiimide (EDC), allowed for the covalent tethering of pre-

synthesized amine-terminated oligonucleotide probes to the PMMA waveguide surface using a non-contact printing system. Through prism coupling, laser light was launched into the waveguide to specifically excite all fluorescent targets properly paired to the probes along the length of the fluidic channel. The ability of this system to detect low abundant DNA point mutations with high diagnostic value was demonstrated by monitoring point mutations in *BRCA*1 genes using a PCR/LDR/addressable zip-code array assay,[21] which we have demonstrated for the detection of point mutations in *K*-ras genes with high diagnostic value for colorectal cancer.[22]

EXPERIMENTAL SECTION

Reagents and materials

PMMA substrates were purchased from Goodfellow (Berwyn, PA). Oligonucleotides were custom-synthesized from Integrated DNA Technologies (Coralville, IA) and were HPLC-purified. EDC and 20× SSC buffer (3 M NaCl, 0.3 M sodium citrate, pH 7) were purchased from Sigma-Aldrich (St. Louis, MO). PCR kits were purchased from Applied Biosystems (Foster City, CA). Other chemicals were of the highest quality available and were obtained from either Sigma-Aldrich or Fisher Scientific (Fair Lawn, NJ) unless otherwise stated. Solutions were prepared with Milli-Q deionized water (18.2 MΩ·cm).

Genomic DNA CRL-2336D, extracted and purified from the breast carcinoma cell line HCC1937 with a known *BRCA*1 mutation genotype, was purchased from ATCC (Manassas, VA). It contained an insertion *C* mutation at nucleotide 5382 of exon 20. Normal tissue adjacent to a human vulva squamous cell carcinoma, which does not contain the 5382 *C* mutation, was a kind gift from Jennifer Zhang (Louisiana State University) and was used as the wild-type sample. Genomic DNA was extracted according to the protocol from the GenElute mammalian genomic DNA miniprep kit from Sigma.

Fabrication of waveguide-embedded microfluidic chip

A single-step, double-sided hot-embossing method was utilized to replicate the fluidic network and the waveguide from two mold masters. Two brass molding tools were fabricated by direct milling using a Kern MMP 2522 micromilling machine (Kern Micro- und Feinwerktechnik GmbH & Co., Murnau, Germany) using a solid carbide end mill. Figure 1A shows the double sided embossing process in which one mold tool defined the air-embedded waveguide and another, the fluidic channel network (see Figure 1B). The waveguide and microchannel patterns were transferred from the molding tools to a piece of 1 mm thick PMMA by hot-embossing using a Jenoptik HEX02 hot-embossing machine (Jena, Germany). Precise alignment of the top and bottom inserts was performed by passive alignment to achieve alignment accuracy of ±20 μm.[23] The molding tools were heated to 165°C and pressed into the PMMA substrate with a force of 20 kN for 2 min. Different embossing conditions were employed to control the waveguide thickness. Following hot-embossing, the chip was removed and cooled to room temperature. The thin microchannel floor served as the waveguide (see Figures 1C and 1D). The embossed chips were then cut into a size of 25 × 75 mm. A single wafer had 9 microfluidic devices with a microchannel width ranging from 300 μm to 1,000 μm and a depth of 50 μm (see Figure 1B). At both ends of the channel were placed 500 μm diameter reservoirs for introducing liquids.

PCR amplification of genomic DNA

Fifty μL of a PCR mixture contained 10 mM Tris-HCl (pH 8.0), 50 mM KCl, 2.5 mM $MgCl_2$, 200 μM dNTPs, 0.4 μM forward primer and 0.4 μM reverse primer (see Table 1 for sequences), 1.25 units AmpliTaq gold hot-start DNA polymerase (Applied Biosystems) and 50 ng of genomic DNA isolated from the appropriate cell line. Upon denaturation at 94°C for

5 min, amplification was achieved by performing 30 cycles at 94°C for 20 s, 65°C for 15 s, 72°C for 15 s, and a final extension at 72°C for 5 min in an Eppendorf Mastercycler (Brinkman Instruments Inc., Westbury, NY). To check PCR integrity, the PCR products were electrophoresed using 4% agarose gels that were stained with ethidium bromide (Cambrex, Rockland, ME) and visualized by UV shadowing. The DNA concentration was determined using absorbance at 260 nm. The PCR products were stored at −20°C.

LDR of BRCA1 samples

LDRs were performed in the same thermocycler as used for PCR in a 20 μL mixture containing 20 mM Tris-HCl (pH 7.6), 25 mM KAc, 10 mM $Mg(Ac)_2$, 10 mM DTT, 1 mM NAD (a cofactor), 0.1% Triton X-100, 30 nM discriminating primers, 30 nM Alexa Fluor 660-labeled common primer, a 1 pmol mixture of PCR products consisting of mutant and/or wild-type DNA and 40 units of *Taq* DNA ligase (New England Biolabs, Beverly, MA). The concentration ratio of mutant:wild-type DNA was adjusted from 0:1 to 1:500. The LDR thermal reaction profile was; 2 min at 94°C; 30 cycles at 94°C for 30 s and 65°C for 2 min.

Oxygen-plasma treatment of PMMA

Following embossing and prior to thermal assembly of the cover plate to the substrate, the PMMA microchannels were rinsed with isopropanol and ddH_2O, dried with air and irradiated with an oxygen plasma using a Technics Series 800 Micro Reactive Ion Etcher (Surplus Process Equipment Corp., Santa Clara, CA). The oxygen pressure was set to 250 mTorr and the radio-frequency (RF) was 50 W. A 2 min exposure was used for all samples.

Measurement of the surface density of carboxylates

The surface density of carboxylate groups on the PMMA surface was determined by the electrostatic interaction between crystal violet (cationic dye) and the carboxylate groups when placed in a basic solution.[24] The PMMA substrates were placed in a crystal violet solution (1 mM in 0.01 N NaOH) for 5 min, and following a thorough water wash, the substrates were immersed in 80% ethanol and then in 0.10 M HCl (80:20, water:ethanol). The surface-confined crystal violet released from the PMMA surface and into the ethanol solutions was combined and the absorbance was then measured. From a calibration plot, the concentration of surface-bound crystal violet was determined and upon normalizing for surface area of the PMMA, the surface coverage of carboxylic acids was calculated (assuming a 1:1 binding stoichiometry).[25]

Immobilization of zip-code probes to PMMA waveguides

The plasma-irradiated microchannel/waveguide was soaked in 200 μg/μL EDC dissolved in a coupling buffer consisting of 0.05 M 2-(*N*-morpholino)ethanesulfonic acid (MES, pH 5.2) and 0.05% proclin-300 obtained from Bangs Laboratories Inc. (Fishers, IN) for 2 min. The channel was then dried under nitrogen. Next, 25 μM 3′-amine-modified oligonucleotide probes (zip-code probes 1, 3, and 11 dissolved in the coupling buffer, see Table 1 for sequences of these probes) were dispensed inside the activated PMMA channel using a PerkinElmer Piezorray non-contact microarray printing system (Downers Grove, IL). Dispensing volumes *per* spot were 0.33 ±0.03 nL and the spot size was 150 μm in diameter. After spotting, the chips were incubated at 37°C for 1 h and washed with 0.1% SDS to remove excess oligonucleotides and finally dried with compressed nitrogen gas. Capping of residual PMMA carboxylate groups was not required.

In-channel flow-through hybridization

A PMMA cover plate of 250 μm thick was thermally annealed onto the zip-code-tethered microchip containing the waveguide in a convection oven at 107°C. A capillary (75 μm i.d.,

363 μm o.d., and 10 cm long; Polymicro Technologies, Phoenix, AZ) was then sealed to the chip reservoirs using epoxy to aid in solution transport. A Pico Plus syringe pump (Harvard Apparatus, Holliston, MA) was used to drive the solution containing the LDR cocktail in hybridization buffer (6× SSC, 0.1% SDS) through the microfluidic assembly. The hybridization was carried out at a flow rate of 2 μL/min (37 ±0.2°C) for 5 min. Following hybridization, the PMMA channels were washed with buffer (2× SSC, 0.1% SDS).

Evanescent-field fluorescence microscope for microarray imaging

Figure 2 shows the microscope used to launch the excitation light into the PMMA waveguide and collect the resulting fluorescence. A 5 mW 675 nm diode laser (Edmund Optics, Barrington, NJ) mounted on a goniometer and micro-translational stage was passed through a line filter (Omega Optical, Brattleboro, VT). The laser light was expanded in one dimension to match the width of the planar waveguide channel. It was coupled into the waveguide using an equilateral PMMA prism placed directly on the PMMA cover plate. A drop of refractive index oil was used for producing complete contact between the chip and coupling prism. The incident angle of the laser beam with respect to the planar waveguide was adjustable through the goniometer. The fluorescence emission was collected using either a 1.25× (N.A. = 0.04) or 10× (N.A. = 0.25) objective and then filtered using a 690 nm long-pass filter (Omega Optical). Using the 1.25× objective, the imaging area (field of view, FOV) was 20 mm (diameter) with a spatial resolution of 16 μm and the 10× objective provided a spatial resolution of 2 μm with a FOV = 2.5 mm.

The fluorescence image was read out with a Photometrics Cascade 1K CCD (Roper Scientific, Tucson, AZ). The CCD was configured in a 1004 *x* 1002 imaging array with the pixel size being 8 μm. Images from the microarray were acquired using MetaMorph software (Version 6.2r6, Universal Imaging Corp., Downingtown, PA) provided with the camera and were analyzed using ScanArray Express software from PerkinElmer. The adaptive circle quantitation method was utilized to fit all spots in the image with circles. Spot signal intensities were determined as mean values of the pixels located within the spot after subtraction of the mean background. The background for each fluorescence spot was determined from a software-generated ring area outside the spot.

RESULTS AND DISCUSSION

Functionalization of PMMA waveguide surfaces with oxygen plasma

As noted, waveguides must possess two operational characteristics when coupled to microarrays; (1) support total internal reflection with a strong evanescent field and; (2) a functional surface that can be used for the covalent attachment of molecular recognition elements. Oxygen plasma was used in this study to modify the PMMA surfaces to produce functional scaffolds (*i.e.*, carboxylates) that could be used for covalently attaching the recognition probes to the waveguide surface.[17, 25, 26]

Because photochemical or plasma treatment can induce surface pitting giving rise to scattering centers on the waveguide surface,[27] we examined the plasma-treated PMMA surface using tapping-mode atomic force microscopy (AFM) and compared the surface profiles to native hot-embossed PMMA. Figure S1 in the Supporting Information shows AFM images of the non-treated waveguide surface and a waveguide treated with a 2 min oxygen plasma. A pristine surface of PMMA was found to have a root mean square (RMS) roughness value of 16.7 ±1.0 nm while the RMS value of the hot-embossed channel was 39.0 ±2.3 nm and that of the plasma irradiated channel 28.6 ±1.8 nm. The channel floor was produced from a raised structure on the top surface of the molding tool and as such, the higher roughness of the embossed PMMA compared to the pristine PMMA results from micro-milling and subsequent lapping steps used

to construct the molding tool. The 2 min plasma oxidation used here was found to reduce this RMS roughness produced by the molding tool. However, longer irradiation times were found to result in significant increases in the RMS roughness values (data not shown).

The electrostatic interactions between crystal violet (a cationic dye) and carboxylates in a basic solution were used to determine quantitatively the surface density of functional groups on PMMA. The average surface density of carboxylates was found to be $2.7 \pm 0.5 \times 10^{-9}$ mol/cm^2, which was higher than 1.4×10^{-9} mol/cm^2 produced using UV irradiation of PMMA.[25]

Fabrication of the waveguides and their operational characteristics

The embossed PMMA core, which serves as the floor of the fluidic channel, forms the waveguide core with the aqueous solution acting as the upper cladding layer and air as the lower and side cladding layers. The force and temperature used for the hot embossing could be adjusted to yield the desired waveguide thickness.

Waveguides require efficient coupling of light into a high-refractive-index core with total internal reflection used to guide the light. From Snell's law, the critical angle for light propagating in the guiding material is calculated from;

$$\theta_{12}=\sin^{-1}(n_2/n_1) \quad (1)$$

where n_1 is the refractive index of the guiding material and n_2 is the refractive index of the cladding. The critical angles for light propagating from PMMA (n_1 = 1.49) to air (n_2 = 1.00) and from PMMA to solution (n_2 = 1.33) were calculated to be 42° and 63°, respectively. A prism was used to couple the laser into the waveguide by adjusting the incident angle using a goniometer (see Figure 2) to launch the light near the critical angle in order to maximize the amount of light coupled into the evanescent field.[15, 28] In addition, the laser light was slightly uncollimated to produce uniform intensity down the length of the waveguide.

To evaluate the transmission efficiency of the laser light (675 nm) per unit length of the guiding medium, the laser output energy was evaluated using waveguides cleaved at different lengths (6 separate measurements). The propagation loss per unit length (PL, db/cm) was calculated using;

$$PL=\frac{10\log(I_1/I_0)}{l} \quad (2)$$

where I_0 and I_1 represent laser energies at the input of the waveguide and at a certain propagation distance (l) from the input, respectively. The propagation loss was found to be 0.68 ± 0.05 dB/cm (6 separate measurements), which is comparable to values reported for other microfabricated polymer waveguides.[29]

An image of nucleic acid probes bearing fluorescent reporters and covalently attached to the PMMA waveguide is shown in Figure 3. A typical fluorescence image of the array is shown in Figure 3A with a contour intensity plot of a single spot shown in Figure 3B. The spot profile demonstrated a nearly flat top indicating uniformity in the functional group production and the evanescent field across a single spot. Inspection of the entire array (~4.5 mm total length) indicated homogeneous irradiation of all probes. In addition, the image did not show evidence of bright spots in non-probe areas, which would be indicative of scattering centers due to surface roughness or refractive inhomogeneity in the bulk material that may have been caused by the embossing process.

The effects of waveguide thickness on the evanescent fluorescence signal and background (signal-to-background ratio, S/B) were then evaluated by spotting a 1 μM solution of the dye-labeled oligonucleotides (see Table 1) into the PMMA channel with different waveguide thicknesses. Figure 4 shows the results of these studies. As can be seen, thinner waveguides produced larger S/B ratios due to more internal reflections *per* unit length producing a higher absolute power coupled into the evanescent field. The ability to make waveguides thinner than ~150 μm was limited by the mechanical stability of the air-suspended guiding medium; waveguides less than 150 μm in thickness typically resulted in severe sagging. Hence, 150 μm thick waveguides were adopted throughout these experiments.

For the spot shown in Figure 3B, the background-corrected integrated fluorescence intensity was found to be 2.9×10^9 CCD counts while the background counts over the same area was 2.8×10^4 CCD counts. If it is assumed that the oligonucleotide-to-surface carboxylate binding ratio is 1-to-1, then the mass detection limit for this waveguide sensor would be 1.8 fmol (SNR = 3). However, this should be taken as an upper limit to the mass detection limit estimate, because the loading level of oligonucleotides to the functionalized PMMA surface is well below that of the surface carboxylate concentration.[17] Because we are already operating at the saturation level of this 16-bit CCD camera, improvements in mass sensitivity could be realized using higher quality polymeric material for the waveguide or improved optical filtering in the optical train to reduce the background level.

Detection of BRCA1 mutations using microfluidics and planar waveguides

For each zip-code probe, a 2 *x* 2 pattern (four replicate spots) were produced using non-contact printing on the plasma-activated planar waveguide to minimize surface damage to the PMMA waveguide. Following probe printing, the microchips containing the waveguides were enclosed with a cover plate using a thermal annealing process to allow microfluidic addressing of the array.

Mutations within the *BRCA*1 gene account for an inherited predisposition to breast cancer, including approximately one-half of families with multiple cases of breast cancers and about 8–10% of women with early-onset breast cancer.[30, 31] PCR amplified products from exon 20 of the HCC1937 breast cancer cell line possess an insertion *C* residue at nucleotide 5382 of this gene.[32] This mutation was used as the model system for testing the performance of the integrated waveguide sensor microfluidic chip using a PCR/LDR/universal array assay.

Each zip-code probe in this study had a 3′-terminus appended with a 15 dT spacer to improve probe accessibility, with an amine functional group for tethering the zip-code probe to the plasma oxidized PMMA surface. As for the LDR, the allele-specific discriminating primers for the mutant DNA contained a zip-code complement (cZip) sequence at its 5′-terminus and a 3′-terminus containing a C quartet (cZip 11-discriminating primer, see Table 1). The discriminating primer for wild-type DNA had a 3′-terminus with a C triplet (cZip 1-wild-type primer). Only one common primer was needed, which had a 5′-terminus that was phosphorylated and a 3′-terminus that was tagged with Alexa Fluor 660. LDR products generated from successful allele-specific ligations using a set of primers (one cZip 11-discriminating primer and one common primer) in the presence of mutant and wild-type DNA were verified using capillary electrophoresis (see Figure S2 in Supporting Information).

Figure 5 shows the results of a continuous-flow assay of LDR products hybridized to zip-codes 11, 1, and 3, which were preformed in a waveguide channel of 1 mm width with each zip code probe patterned in a 2 *x* 2 format. Zip-code probe 3 was not complementary to either the mutant or wild-type DNA targets and was therefore selected as the control. No fluorescence was seen from any of the zip-code 3 probes. Also, no fluorescence was discernible in the image when no DNA substrate (mutant or wide-type template) was placed in the LDR cocktail (image A

in Figure 5). When only wild-type DNA was added into the LDR cocktail, matched wild-type LDR products were produced as seen by the corresponding signal generated at zip-code 1 (see image B of Figure 5). When only mutant DNA was placed in the LDR cocktail, large amounts of matched products were produced showing high fluorescence intensity for zip-code probe 11 (image C in Figure 5). When the LDR contained low abundant *BRCA*1 mutations (1% or 10% mutant) in the presence of large amounts of wild-type sequences, matched wild-type and mutant LDR products were generated and hybridized to their appropriate zip-code probes (see images D and E in Figure 5).

CONCLUSIONS

We have developed a waveguide-embedded microfluidic chip in a single fabrication step using double-sided hot-embossing. The waveguide was air-embedded along three sides and in-contact with the sampling solution on the forth side (floor of the microfluidic channel). The PMMA waveguide could be treated with oxygen-plasma to generate a functional scaffold to which non-contact micro-dispensed amine-terminated oligonucleotide probes could be covalently attached using EDC coupling chemistry. The system was successfully tested by building low-density universal zip-code arrays for detecting point mutations in *BRCA1* genes using an allele-specific ligation assay. The alleviation of multiple fabrication steps typically required to build waveguides integrated into fluidic systems will provide a venue for creating inexpensive devices that can be used in a disposable format for *in vitro* molecular diagnostics. Evanescent excitation of the low-density array along with microfluidic addressing was capable of collecting the hybridization signatures from the microarray in as little as ~5 min (includes hybridization and imaging times).

Supplementary Material

Refer to Web version on PubMed Central for supplementary material.

Acknowledgements

We thank Dr. Wayne Zhou and Jennifer Zhang for providing DNA samples and Thaya Guedry, Jason Guy, Dr. Guofang Chen, Zhiyong Peng, Dr. Catherine Situma, and Jason Emory for technical assistance and discussions. We are grateful for the financial support of this work from the National Science Foundation (EPS-0346411), the National Institutes of Health (EB002115, CA0099246) and the State of Louisiana Board of Regents.

References

1. Schena, M. Microarray Biochip Technology. Eaton Publishing; Natick, MA: 2000.
2. Yang P, Wirnsberger G, Huang HC, Cordero SR, McGehee MD, Scott B, Deng T, Whitesides GM, Chmelka BF, Buratto SK, Stucky GD. Science 2000;287:465–467. [PubMed: 10642543]
3. Barnes WL, Dereux A, Ebbesen TW. Nature 2003;424:824–830. [PubMed: 12917696]
4. Arentoft J, Sondergaard T, Kristensen M, Boltasseva A, Thorhauge M, Frandsen L. Electron Lett 2002;38:274–275.
5. Pawlak M, Schick E, Bopp MA, Schneider MJ, Oroszlan P, Ehrat M. Proteomics 2002;2:383–393. [PubMed: 12164697]
6. Sugimoto Y, Tanaka Y, Ikeda N, Nakamura Y, Asakawa K, Inoue K. Opt Express 2004;12:1090–1096.
7. Kawakami S. Electron Lett 1997;33:1260–1261.
8. Papra A, Bernard A, Juncker D, Larsen NB, Michel B, Delamarchce E. Langmuir 2001;17:4090–4095.
9. Plowman TE, Durstchci JD, Wang HK, Christensen DA, Herron JN, Reichert WM. Anal Chem 1999;71:4344–4352. [PubMed: 10517150]
10. Adar R, Serbin MR, Mizrahi V. J Lightwave Technol 1994;12:1369–1372.

11. Rowe CA, Tender LM, Feldstein MJ, Golden JP, Scruggs SB, MacCraith BD, Cras JJ, Leigler FS. Anal Chem 1999;71:3846–3852. [PubMed: 10489530]
12. Reichert WM, Ives JT, Suci PA, Hlady V. Appl Spectrosc 1987;41:636–640.
13. Ives JT, Reichert WM. Appl Spectrosc 1988;42:68–72.
14. Shadpour H, Musyimi H, Chen JF, Soper SA. J Chromatogr A 2006;1111:238–251. [PubMed: 16569584]
15. Chronis N, Lee LP. Lab Chip 2004;4:125–130. [PubMed: 15052352]
16. Situma C, Hashimoto M, Soper SA. Biomol Eng 2006;23:213–231. [PubMed: 16905357]
17. Wang Y, Vaidya B, Farquar HD, Stryjewski W, Hammer RP, McCarley RL, Soper SA, Cheng YW, Barany F. Anal Chem 2003;75:1130–1140. [PubMed: 12641233]
18. Liu RH, Yang JN, Lenigk R, Bonanno J, Grodzinski P. Analytical Chemistry 2004;76:1824–1831. [PubMed: 15053639]
19. Liu YJ, Rauch CB, Stevens RL, Lenigk R, Yang JN, Rhine DB, Grodzinski P. Anal Chem 2002;74:3063–3070. [PubMed: 12141665]
20. Anderson RC, Su X, Bogdan GJ, Fenton J. Nucleic Acids Res 2000;28:e60. [PubMed: 10871383]
21. Favis R, Day JP, Gerry NP, Phelan C, Narod S, Barany F. Nat Biotechnol 2000;18:561–564. [PubMed: 10802632]
22. Hashimoto M, Hupert ML, Murphy MC, Soper SA, Cheng YW, Barany F. Anal Chem 2005;77:3243–3255. [PubMed: 15889915]
23. Datta P, Xu F, Gurung S, Soper SA, Goettert J. Proc SPIE 2005;6112:611208.
24. Rivaton A. Polym Degrad Stab 1995;49:163–179.
25. McCarley RL, Vaidya B, Wei S, Smith AF, Patel AB, Feng J, Murphy MC, Soper SA. J Am Chem Soc 2005;127:842–843. [PubMed: 15656615]
26. Hashimoto M, Barany F, Soper SA. Biosen & Bioelectr 2006;21:1915–1923.
27. Wei SY, Vaidya B, Patel AB, Soper SA, McCarley RL. J Phys Chem B 2005;109:16988–16996. [PubMed: 16853163]
28. Taitt CR, Anderson GP, Ligler FS. Biosen & Bioelectr 2005;20:2470–2487.
29. Kim JS, Kim JJ. IEEE Photonics Technology Letters 2004;16:798–800.
30. FitzGerald MG, MacDonald DJ, Krainer M, Hoover I, O'Neil E, Unsal H, Silva-Arrieto S, Finkelstein DM, Beer-Romero P, Englert C, Sgroi DC, Smith BL, Younger JW, Garber JE, Duda RB, Mayzel KA, Isselbacher KJ, Friend SH, Haber DA. N Engl J Med 1996;334:143–149. [PubMed: 8531968]
31. Langston AA, Malone KE, Thompson JD, Daling JR, Ostrander EA. N Engl J Med 1996;334:137–142. [PubMed: 8531967]
32. Tomlinson GE, Chen TT, Stastny VA, Virmani AK, Spillman MA, Tonk V, Blum JL, Schneider NR, Wistuba II, Shay JW, Minna JD, Gazdar AF. Cancer Res 1998;58:3237–3242. [PubMed: 9699648]

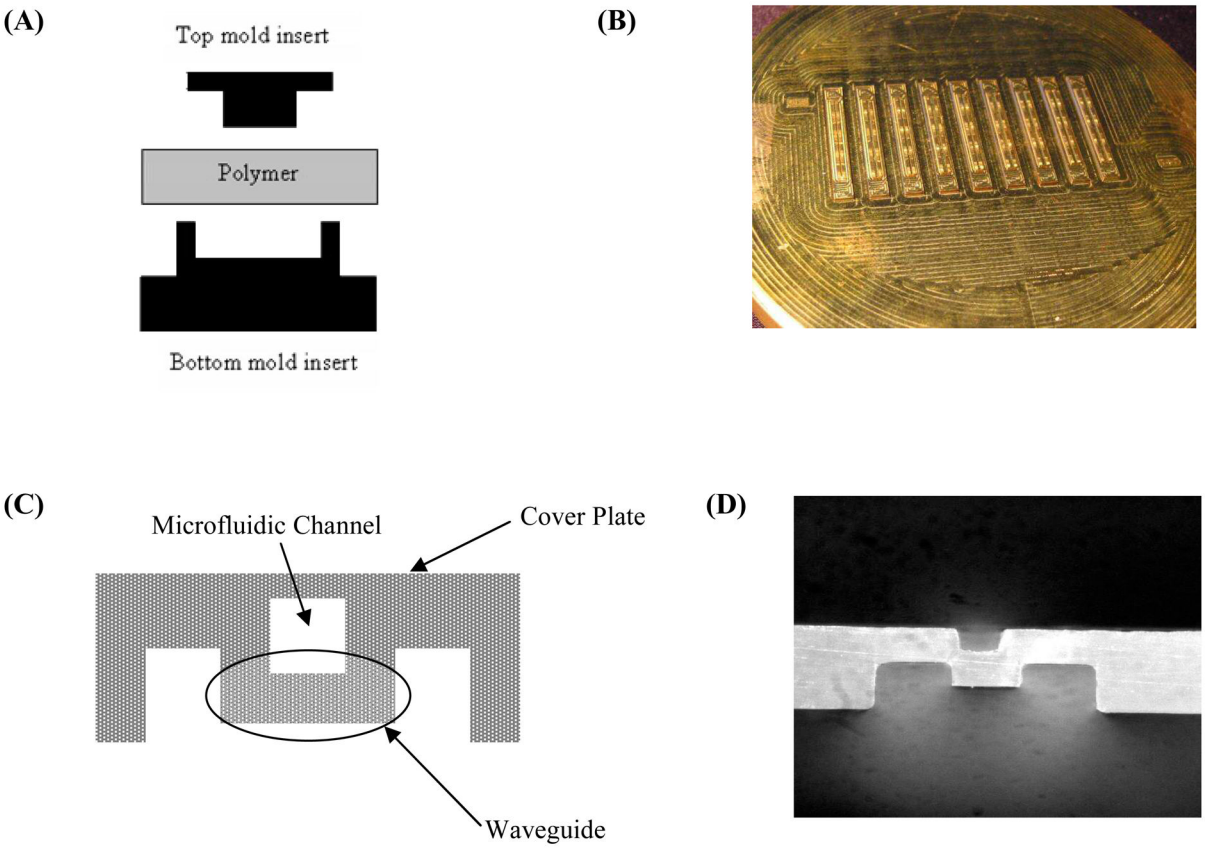

Figure 1.
Schematic diagram of the double-sided hot-embossed PMMA microchips with embedded waveguides. (A) Schematic showing the double-sided, hot-embossing in which two brass molding tools were used to fabricate the microfluidic chips with integrated waveguides. (B) Picture of a brass molding tool fabricated by the micromilling technique showing the fluidic network. Nine different chips were produced from a single hot-embossing step. (C) Cross sectional view of the waveguide-based microchip. (D) Optical micrograph of a cross sectional view of the embossed waveguide and microfluidic channel. The channel floor acts as the core layer of the waveguide onto which microarray spots were dispensed.

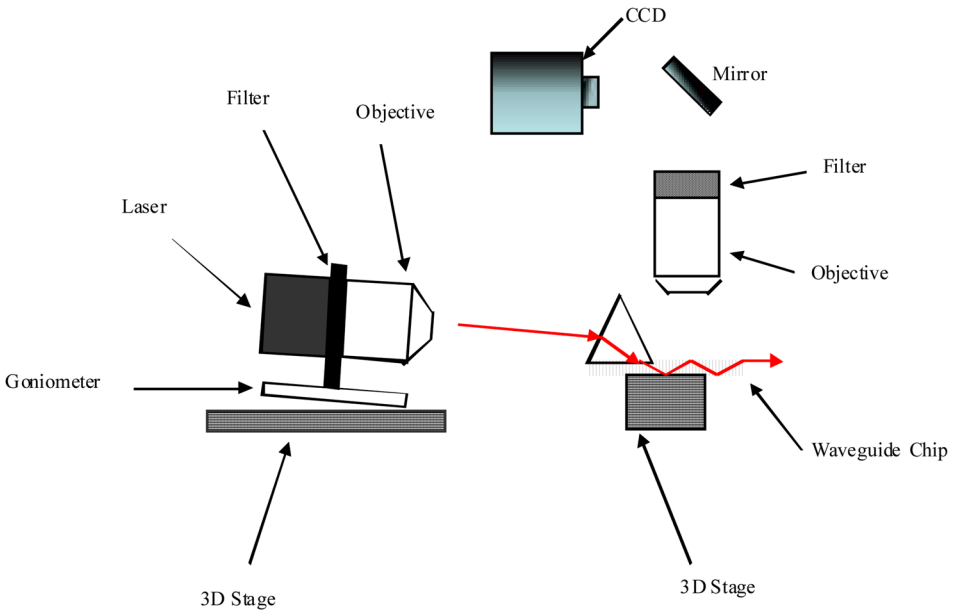

Figure 2.
Diagram showing the evanescent-field fluorescence microscope used to launch the laser light into the integrated microfluidic PMMA planar waveguide chip and collect the resulting fluorescence. The uncollimated light from a diode laser (675 nm) was coupled into the PMMA waveguide using prism coupling. The evanescent field of the waveguide was used to excite fluorescence at the polymer/solution interface. The evanescently excited fluorescence was collected with an objective, passed through a 690 nm long-pass filter and imaged onto a CCD camera.

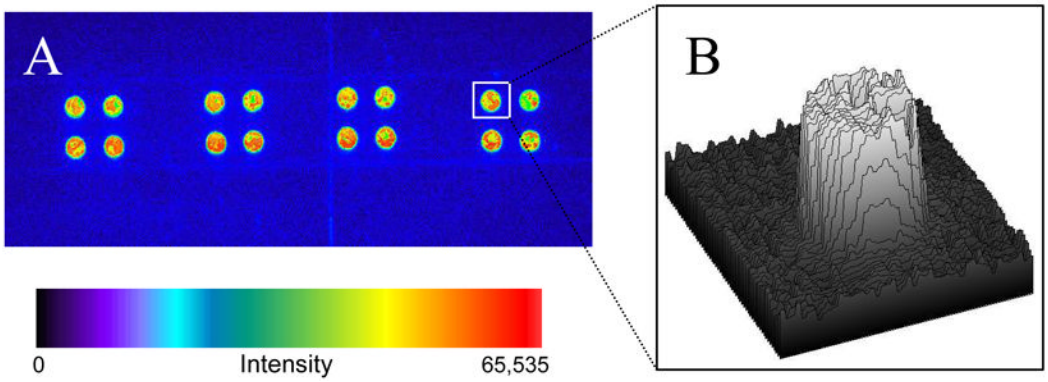

Figure 3.

(A) Analysis of Alexa Fluor 660-labeled oligonucleotide probes (1 μM) spotted into a 500 μm wide channel (spot diameter = 150 μm) with a waveguide thickness of 150 μm using the marker oligonucleotide (see Table 1). The waveguide channel was irradiated by oxygen plasma for 2 min, activated with EDC and incubated with the fluorescently-labeled marker oligonucleotide probes. The excess probes were washed with 0.1% SDS and detected using evanescent excitation and imaged onto a CCD through a 1.25× objective with an exposure time set to 5 s. (B) Contour plot showing the fluorescence intensity distribution of a single probe spot. The image shown in (B) represents a spot ~4.0 mm down the length of the waveguide from the input end. The lighter intensity horizontal lines in the image of (A) represent the fluidic channel walls. The intensity scale (false-color image) is denoted by the color bar and represents CCD counts.

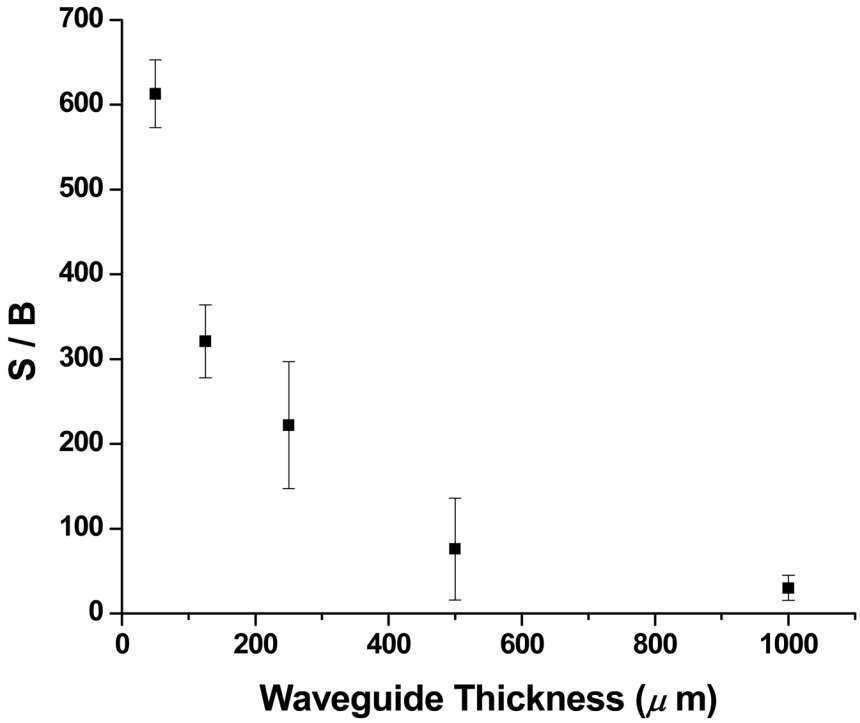

Figure 4.

Signal-to-background (S/B) ratio as a function of PMMA waveguide thickness. The error bars represent one standard deviation, which were determined from triplicate measurements. The S/B ratios were determined by spotting the marker oligonucleotides onto the waveguides and imaged for 5 s using the CCD (1.25× objective used for collecting the resulting fluorescence). See Figure 3 for experimental details.

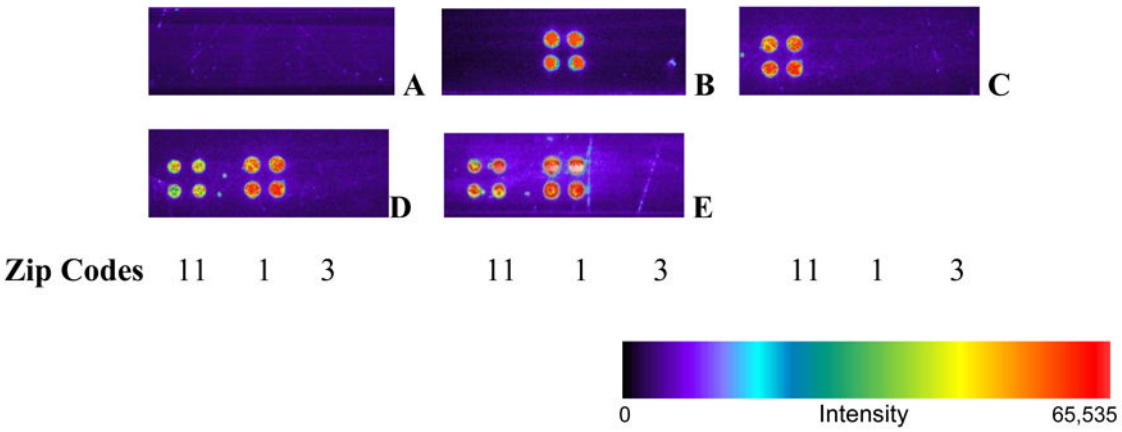

Figure 5.

False-color images of zip-code microarrays used for the detection of insertion *C* mutations in the *BRCA*1 gene at different mutant:wild-type ratios using the microfluidic device with an embedded waveguide. There were three sets of probes (25 μM zip-code probes 11, 1, and 3) to interrogate mutant, wide-type and negative control DNAs, respectively. Each zip-code probe was spotted in quadruplicate (diameter = 150 μm, pitch = 240 μm). The LDR products were diluted in hybridization buffer (6× SSC, 0.1% SDS) and flowed through the microchannels at a flow rate of 2 μL/min (37°C hybridization temperature). After the 5-min hybridization, the channels were rinsed with a wash solution (2× SSC - 0.1% SDS) at 2 μL/min for 2 min and imaged using the evanescent-field fluorescence microscope with a 5 s exposure time (1.25× objective for image capture). Each LDR reaction used two discriminating primers (one for mutant allele and one for the wild-type allele) and one common primer. Image A: LDR with no DNA template (negative control 1); image B: LDR with wide-type template only (negative control 2); image C: LDR containing the mutant template only; image D: LDR containing a mixture of 1% mutant template and 99% wide-type template; image E: LDR containing a mixture of 10% mutant template and 90% wide-type template.

Table 1

Oligonucleotide sequences used for the PCR/LDR/zip-code hybridization assays interrogated using the planar waveguide and imaging microscope. The zip-code probes (1, 3, 11) and the complement zip-codes carried on the discriminating LDR primers are given in lower-case letters. The marker oligonucleotide was spotted directly onto the activated PMMA surface and interrogated using fluorescence evanescent excitation without hybridization to a solution complement.

Oligonucleotide	**sequence (5′→3′)**	T_m **(°C)**
*BRCA*1 exon 20 forward primer	AGG AGA TGT GGT CAA TGG AAG AAA	56.2
*BRCA*1 exon 20 reverse primer	GAA TAC AGA GTG GTG GGG TGA GAT	58.1
LDR cZip11-discriminating Primer	cgc aag gta ggt gct gta ccc gca CAA AGC GAG CAA GAG AAT CCC C	71.7
LDR cZip1-discriminating Primer	gct gag gtc gat gct gag gtc gca CAA AGC GAG CAA GAG AAT CCC	71.0
LDR common Primer	*P* AGG ACA GAA AGG TAA AGC TCC CTC-F	58.2
zip-code 1	tgc gac ctc agc atc gac ctc agc-sp-amine	64.4
zip-code 3	cag cac ctg acc atc gat cgc agc-sp-amine	63.9
zip-code 11	tgc ggg tac agc acc tac ctt gcg-sp-amine	64.7
Marker	F-GTA AAA CGA CGG CCA GT-sp-amine	52.6

p phosphorylated; F=Alexa Fluor 660 (Ex/Em = 663 nm/690 nm); sp-amine =-$(T)_{15}(CH_2)_6NH_2$.